

Article

Real-Time Sea State Estimation for Wave Energy Converter Control via Machine Learning

Tanvir Alam Shifat ¹, Ryan Coe ², Gioegio Bacelli ² and Ted Brekken ^{1,*}

¹ School of Electrical Engineering & Computer Science, Oregon State University, Corvallis, OR 97331, USA; shifatt@oregonstate.edu

² Water Power Technologies Department, Sandia National Laboratories, Albuquerque, NM 87185, USA; rcoe@sandia.gov (R.C.); gbacell@sandia.gov (G.B.)

* Correspondence: brekken@eecs.oregonstate.edu; Tel.: +1-541-737-2995

Abstract: Wave energy converters (WECs) harness the untapped power of ocean waves to generate renewable energy, offering a promising solution to sustainable energy. An optimal WEC control strategy is essential to maximize power capture that dynamically adjusts system parameters in response to rapidly changing sea states. This study presents a novel control approach that leverages neural networks to estimate sea states from onboard WEC measurements such as position, velocity, and force. Using a point absorber WEC device as a test platform, our proposed approach estimates sea states in real-time and subsequently adjusts PID controller gains to maximize energy extraction. Simulation results across diverse sea conditions demonstrate that our strategy eliminates the need for external wave monitoring equipment while maintaining power capture efficiency. The results show that our neural network-based control technique can improve power capture by 25.6% while significantly reducing system complexity. This approach offers a practical alternative for WEC deployments where direct wave measurements are either infeasible or cost prohibitive.

Keywords: wave energy converter (WEC); sea state estimation; machine learning; PIDcontrol



Academic Editor: José A. Orosa

Received: 29 March 2025

Revised: 6 May 2025

Accepted: 12 May 2025

Published: 21 May 2025

Citation: Shifat, T.A.; Coe, R.; Bacelli, G.; Brekken, T. Real-Time Sea State Estimation for Wave Energy Converter Control via Machine Learning. *Appl. Sci.* **2025**, *15*, 5772. <https://doi.org/10.3390/app15105772>

Copyright: © 2025 by the authors. Licensee MDPI, Basel, Switzerland. This article is an open access article distributed under the terms and conditions of the Creative Commons Attribution (CC BY) license (<https://creativecommons.org/licenses/by/4.0/>).

1. Introduction

Harnessing ocean wave energy offers a promising renewable energy resource by exploiting the vast and consistent energy of the ocean. Wave energy converters (WECs) face significant challenges in achieving efficient energy conversion due to the dynamic and unpredictable nature of ocean waves [1]. Effective control strategies are crucial to ensure that WECs operate optimally and safely under these varying conditions, although developing such strategies is a challenging task.

Several types of WEC control strategies have been widely explored in the literature. These strategies mainly utilize predefined incoming ocean wave characteristics to optimize control actions and maximize energy extraction. Model predictive control (MPC) is a popular approach for WECs when wave profiles are known, and it can be used in diverse sea state conditions while obeying system constraints. Fusco and Ringwood [2] introduced an MPC framework that used wave profile information to optimize Power Take-Off (PTO) forces for enhanced energy absorption. Similarly, Henriques et al. [3] demonstrated simplified wave models for MPC, improving real-time performance. Complex conjugate control (CCC) maximizes power transfer by matching the impedance of the WEC to the incoming wave. Foundational work by Falnes [4] showed that known wave excitation forces allow impedance matching for optimal energy transfer. However, CCC is non-causal,

as it requires future knowledge of wave forces. Li and Belmont [5] developed predictive approximations to make CCC viable in real-time applications. Feedback resonating control (FBR) tested by Coe et al. [6] shows promising results by leveraging known sea states to adjust resonance frequencies. Proportional–integral–derivative (PID) controllers, often adapted with wave prediction, have also been studied in the WEC context. Yu and Falnes [7] demonstrated that PID control tuned to anticipated wave periods and amplitudes allowed WECs to track wave oscillations effectively. Adaptive PID gains, as seen in the work of Vantorre et al. [8], further improved performance over short intervals as wave conditions varied. In parallel, classical state-estimation algorithms such as Kalman filtering [9], the Extended Kalman Filter (EKF) [10], and the Unscented Kalman Filter (UKF) [11] have long been used to infer unmeasured dynamic states under linear or mildly nonlinear models and Gaussian noise assumptions. Particle filters [12] generalize this to highly nonlinear, non-Gaussian settings via sequential Monte Carlo sampling. In the WEC domain, Coe et al. [6] demonstrated a Kalman-based wave-prediction scheme to infer excitation forces from onboard measurements, though its accuracy degrades under model mismatch and non-Gaussian disturbances. Linear quadratic regulator (LQR) controllers [13] optimize a quadratic cost around a fixed linearization, requiring re-linearization or gain scheduling as sea conditions change. A central assumption for these approaches is to have a well-defined model representation of the WEC device, which is often computationally expensive given diverse sea conditions.

Machine learning techniques, particularly deep learning, have recently emerged as promising tools for WEC control due to their adaptability and ability to generalize across diverse conditions [14,15]. In wave energy research, deep neural networks (DNNs) have been explored for predicting wave characteristics based on historical data and WEC operational parameters [16]. These studies suggest that DNNs can be effective in identifying patterns in highly variable data, enabling WECs to respond more flexibly to changing ocean states without direct wave measurements. More recently, reinforcement learning has been applied to optimize control based on known sea states. Duarte and Sarmiento [17] developed a reinforcement learning-based controller trained on wave data, predicting control actions across various sea states. These methods show promise but require extensive training data and computational resources, limiting practical WEC deployment in real ocean environments. Despite control approaches from different angles, estimating incoming wave or sea state from the physical measurements of the WEC device remains limited.

Despite these advancements, most WEC control strategies rely on direct wave measurements using buoys, radar, or pressure sensors to optimize power capture. But these approaches are costly, maintenance intensive, and vulnerable to harsh marine conditions. Real-time data acquisition also introduces latency and communication constraints, limiting its effectiveness for dynamic control. Moreover, wave sensors can fail or become impractical in extreme environments, making them unreliable for long-term deployment. These challenges highlight the need for an alternative approach that eliminates dependence on external wave measurements. Machine learning, particularly deep learning, offers a potential solution by extracting meaningful patterns from these onboard measurements. Neural networks have shown success in renewable energy applications [14], including wave prediction [16], but their use in WEC control remains underexplored. Furthermore, while nonlinear model-based controllers can handle system uncertainties, they require detailed parametric models and the extensive tuning of control parameters, which may be impractical under rapidly changing sea states. Reinforcement-learning-based tuning methods such as DDPG offer end-to-end policy optimization but demand large volumes of training data and online exploration, posing safety and sample-efficiency challenges in marine environments.

To overcome these challenges, we propose a machine learning-based control strategy that estimates sea states directly from onboard WEC measurements (position, velocity, and force), eliminating the need for external wave sensors. In this study, we develop and evaluate a long short-term memory (LSTM)-based control framework that uses physical data from the WEC itself to predict the incoming wave spectrum, aiming to improve energy capture efficiency and device adaptability under real-world conditions. By training and validating the model across a broad range of operational scenarios, we demonstrate how this control strategy enhances WEC performance by making it more responsive and resilient to changing ocean waves. We propose a novel LSTM-based framework for real-time sea-state estimation using only onboard WEC measurements, and integrate this estimator into a supervisory control loop that updates PID gains every 10 s. Through comprehensive simulations, we demonstrate that this adaptive approach achieves a 25.6% increase in power capture under variable sea conditions relative to fixed-gain PI control. Furthermore, we show robustness to model mismatch by employing noise-augmented training during model development. This research contributes to advancing wave energy technology by addressing key limitations in current control strategies, potentially enabling more efficient and sustainable ocean energy solutions.

This paper is structured as follows. Section 2 describes the WaveBot dynamics. Section 3 introduces our LSTM-based estimation framework and supervisory control. Section 4 details the PI-gain design and stability analysis. Section 5 presents the simulation results under fixed and variable seas. Section 6 discusses the implications, and Section 7 concludes.

2. WEC Device

2.1. WaveBot Device Specifications

The WaveBot is a point absorber type of WEC device that operates as a heaving buoy using a PTO mechanism that translates vertical oscillations into rotational energy. This design enables effective energy extraction by directly converting wave motion into electrical power. WaveBot employs a rack-and-pinion mechanism with a high gear ratio, enhancing the rotational velocity transferred to the PTO and maximizing power generation. Essential device specifications are listed in Table 1, which shows the WaveBot's primary components and energy conversion stages. An illustration of the device is shown in Figure 1.

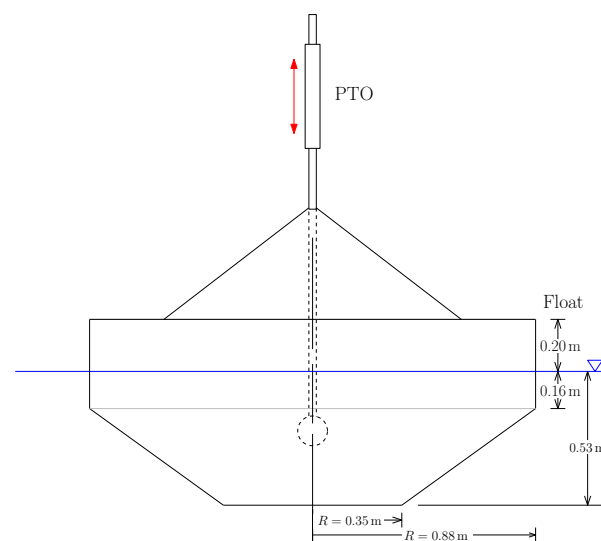


Figure 1. CAD diagram of the WaveBot WEC device [18].

Table 1. WaveBot physical parameters.

Parameter	Value	Unit
Rigid body mass, m	875	kg
Hydrostatic stiffness, k_h	2.44	kN/m
Linear friction coefficient, b_f	1	Ns/m
Gear ratio, N	12.4666	rad/m
Shaft inertia, J_d	2	kg m ²
Torque constant, k_τ	6.1745	Nm/A
Motor winding resistance, R_w	0.5	Ω

2.2. WEC Dynamics

The dynamics of a WEC operating in heave can be described by considering all forces acting on the system as shown in Equation (1):

$$m \cdot a = F_{exc} + F_{rad} + F_{hydro} + F_{fric} - F_{pto} \tag{1}$$

where m is the mass of the WEC, a is the vertical acceleration of the WEC, F_{exc} is the excitation force exerted by incoming ocean waves, F_{rad} is the radiation force modeling the reactive effect of water due to the movement of the WEC, F_{hydro} is the hydrostatic restoring force reflecting the balance of buoyancy and gravity, F_{fric} is the frictional force from internal damping within the WEC system, and F_{pto} is the PTO force, which opposes the motion of the WEC to extract energy [4].

For maximum power absorption, mechanical impedance matching is applied by aligning the PTO impedance $Z_{pto}(\omega)$ with the complex conjugate of the intrinsic mechanical impedance of WEC, $Z_i(\omega)$ [18], where

$$Z_i(\omega) = B(\omega) + b_f + j\left(\omega(m + A(\omega)) - \frac{k_h}{\omega}\right) \tag{2}$$

The WaveBot’s dynamics are driven by a combination of wave excitation forces, PTO forces, and the system’s intrinsic mechanical impedance. The linear equation of motion for vertical displacement in response to wave-induced forces is given by

$$F_{exc}V(\omega) - F_{pto}V(\omega) = Z_iV(\omega) \cdot V(\omega) \tag{3}$$

Here, $B(\omega)$ represents the radiation damping, $A(\omega)$ denotes the added mass, and ω is the angular frequency of the oscillatory motion. This impedance is a function of the device’s hydrodynamic properties and acts as a frequency-dependent resistance to vertical motion. The optimal condition for power transfer is achieved by setting

$$F_{pto, opt}(\omega) = Z_{pto}(\omega)V(\omega) = Z_i^*(\omega)V(\omega) \tag{4}$$

This optimal control law can be approximated in sea states dominated by one frequency as a proportional–integral feedback law

$$F_{pto, opt}(\omega) \approx Z_{pto,PI}(\omega)V(\omega) = \left(K_P + \frac{K_I}{j\omega}\right) V(\omega) \tag{5}$$

To maximize power transfer, we approximate $Z_{pto,PI}(\omega)$ to match $Z_i^*(\omega)$ within the range of frequencies where the wave excitation is significant. This approach results in the following conditions for the PI controller gains:

$$K_P = B(\omega) + b_f \tag{6}$$

$$K_I = \omega^2(m + A(\omega)) - k_h \tag{7}$$

3. Proposed Control Approach

WEC Control by Sea State

WEC control traditionally relies on anticipating and responding to incoming ocean wave to maximize energy capture. In a study by Coe et al. (2018), several WEC control methods are evaluated, including FBR control and MPC [6]. These approaches attempt to match the controller’s response to wave characteristics, often through wave prediction. However, capturing wave profiles directly requires additional equipment like auxiliary measurement buoys, leading to increased complexity, cost, and reliability issues.

In contrast to direct measurement, we propose a control strategy that predicts sea states based on the velocity, position, and PTO force of the WEC device. By analyzing these parameters, our approach identifies the sea state that would produce the observed WEC dynamics, allowing the dynamic selection of optimal control gains. This method leverages readily accessible metrics, eliminating the need for direct wave measurements. The prediction is inherently reactive to the WEC’s real-time response, reducing delay and uncertainty while achieving high energy capture with less complexity.

The proposed WEC control method begins by collecting readily measurable parameters from the WEC, specifically the device’s position (z), velocity (\dot{z}), and the PTO force (F_{PTO}), which are essential indicators of the interaction of the WEC with incoming waves. These parameters are then used as inputs to a neural network model that predicts sea state characteristics, i.e., peak wave period (T_p).

A JONSWAP spectrum in terms of sea states can be expressed as follows:

$$S(\omega) = \frac{\alpha g^2}{\omega^5} \exp\left(-\frac{5}{4}\left(\frac{\omega}{\omega_p}\right)^{-4}\right) \gamma^{\exp\left(-\frac{(\omega-\omega_p)^2}{2\sigma^2\omega_p^2}\right)} \tag{8}$$

where

$$\alpha = \frac{5}{16} \frac{H_m^2}{T_p^4}, \quad \omega_p = \frac{2\pi}{T_p}, \quad \sigma = \begin{cases} 0.07, & \text{if } \omega \leq \omega_p, \\ 0.09, & \text{if } \omega > \omega_p \end{cases}$$

where we have the following: α is the Phillips parameter, controlling the overall amplitude of the spectrum; g is gravitational acceleration; ω is the wave frequency; ω_p is the peak wave frequency; γ is the peak enhancement factor; and σ is the spectral width parameter, with typical values of $\sigma = 0.07$ for $\omega < \omega_p$ and $\sigma = 0.09$ for $\omega \geq \omega_p$.

The neural network model is trained and fine-tuned by incorporating additive white Gaussian noise (AWGN) to improve robustness in noisy conditions. Once the sea state parameter T_p is predicted, it is mapped to obtain optimal controller gains (K_P and K_I) for a PID controller. This enables dynamic adjustment of the control actions to match the identified sea state characteristics and maximize energy absorption. Figure 2 represents the overall proposed approach showing the input excitation force, F_{exec} , and primary and supervisory control blocks to obtain the desired PTO force, F_{PTO}^* . Primary control is the conventional PID control block, which takes peak periods (T_p) of sea states as input. The supervisory control block is the neural network approach that takes features from the WEC

physical parameters and estimates the corresponding T_p . The WEC system was obtained for a sample time of 0.1 s, and hence the step time for both supervisory and primary control blocks is kept at 0.1 s.

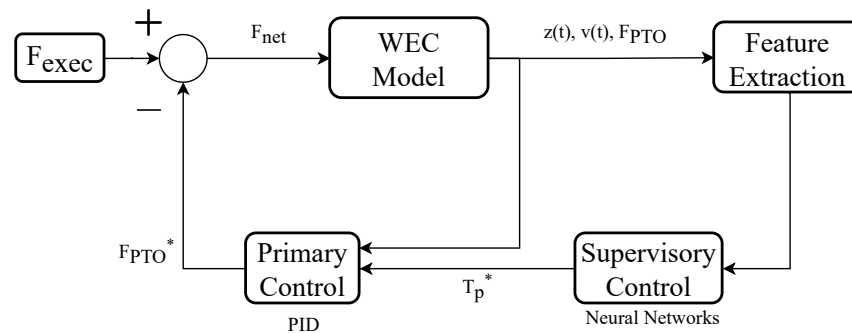


Figure 2. System diagram for sea-state predictive control.

4. Control Design

The primary objective of the WEC control system is to maximize power capture while maintaining stability across varying sea states. In this study, a PI controller is implemented, where the gains K_P and K_I are computed based on the mechanical impedance of the system rather than an optimization-based tuning approach.

The PI controller regulates the response of the WEC to ocean waves, ensuring optimal energy harvesting. The controller transfer function is given by

$$C(\omega; K_P, K_I) = K_P - i \frac{K_I}{\omega}, \tag{9}$$

where K_P and K_I represent the proportional and integral gains, respectively, and $\omega = 2\pi f$ is the angular frequency.

Instead of determining K_P and K_I through numerical optimization, the new approach computes the gains directly from the system’s mechanical impedance. The state-space representation of the WEC device is given by

$$\mathbf{x}[k + 1] = A\mathbf{x}[k] + B\mathbf{u}[k], \tag{10}$$

$$\mathbf{y}[k] = C\mathbf{x}[k] + D\mathbf{u}[k], \tag{11}$$

where $A, B, C,$ and D are the state-space matrices representing the system dynamics.

The mechanical impedance of the WEC is derived from the system’s transfer function. Given a wave period T , the corresponding frequency is $\omega = \frac{2\pi}{T}$.

Using a discrete-time representation, the transfer function $H(z)$ is computed as

$$H(z) = C(zI - A)^{-1}B + D, \tag{12}$$

where $z = e^{j\omega T_s}$ is the discrete-time frequency response variable, and T_s is the sampling time:

$$K_P = \text{Re}(Z_{\text{mech}}^*), \tag{13}$$

$$K_I = -\omega \cdot \text{Im}(Z_{\text{mech}}^*). \tag{14}$$

To ensure stability and prevent extreme values, K_P and K_I are constrained within predefined limits: $K_P \in [0, 5 \cdot 10^3]$, $K_I \in [-2 \cdot 10^4, 1 \cdot 10^6]$. Details on the impedance-based WEC control design, and performance and stability considerations can be found in [6,18].

This method allows for the real-time adaptation of control gains based on sea state variations without requiring iterative numerical optimization, improving computational efficiency and robustness. The implementation is carried out in MATLAB, where the PI gains are computed dynamically based on the measured wave period T_p .

4.1. Neural Network Modeling

In this study, we used a deep learning model named Long Short-Term Memory (LSTM) network, which is a class of recurrent neural networks (RNNs). This model can handle sequential data by addressing the vanishing gradient problem encountered in traditional RNNs. Unlike conventional feedforward neural networks, LSTMs maintain an internal memory state, allowing them to capture long-range dependencies in time-series data. This makes them particularly well suited for problems involving temporal patterns, which is much needed in our study of incoming wave prediction.

As shown in Figure 3, an LSTM cell consists of three primary gates: the forget gate, the input gate, and the output gate, which regulate the flow of information through the network. The LSTM cell updates its cell state C_t and hidden state h_t at each time step t based on the previous hidden state h_{t-1} , the previous cell state C_{t-1} , and the current input x_t . The update process is given by the following equations:

$$f_t = \sigma(W_f x_t + U_f h_{t-1} + b_f) \quad \text{(Forget Gate)} \quad (15)$$

$$i_t = \sigma(W_i x_t + U_i h_{t-1} + b_i) \quad \text{(Input Gate)} \quad (16)$$

$$\tilde{C}_t = \tanh(W_c x_t + U_c h_{t-1} + b_c) \quad \text{(Cell State Candidate)} \quad (17)$$

$$C_t = f_t \odot C_{t-1} + i_t \odot \tilde{C}_t \quad \text{(Cell State Update)} \quad (18)$$

$$o_t = \sigma(W_o x_t + U_o h_{t-1} + b_o) \quad \text{(Output Gate)} \quad (19)$$

$$h_t = o_t \odot \tanh(C_t) \quad \text{(Hidden State Update)} \quad (20)$$

Here, $\sigma(\cdot)$ represents the sigmoid activation function, $\tanh(\cdot)$ is the hyperbolic tangent function, and \odot denotes element-wise multiplication. The weight matrices W_f, W_i, W_c, W_o and U_f, U_i, U_c, U_o along with the biases b_f, b_i, b_c, b_o are learned parameters. LSTMs outperform traditional RNNs in sequence modeling due to their ability to selectively retain or forget information over long sequences. Unlike standard feedforward networks, which process inputs independently, LSTMs utilize a gating mechanism to control information flow, enabling them to learn dependencies over extended time horizons. This is crucial for applications where past inputs influence future predictions, such as ocean wave dynamics. A detailed optimization approach for the LSTM model is presented in Algorithm 1.

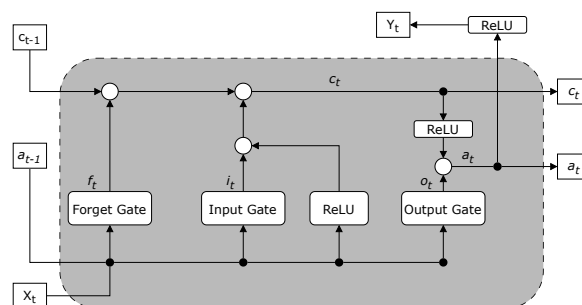


Figure 3. Structure of an LSTM cell, showing the forget, input, and output gates [19].

Algorithm 1 LSTM estimator training and optimization.

Require: Raw WEC data $\mathcal{D} = \{(z_t, \dot{z}_t, F_{PTO,t}, T_{p,t})\}_{t=1}^M$, window length L , learning rate η_0 , max epochs N_{ep}
Ensure: Optimized LSTM parameters θ^*

Data Preparation:

Partition \mathcal{D} into overlapping windows of length L : $\{X^{(i)}, y^{(i)}\}$

Normalize features in $X^{(i)}$ via min–max scaling

Augment: $X^{(i)} \leftarrow X^{(i)} + \mathcal{N}(0, \sigma_{\text{noise}}^2)$

Split into training, validation, and test sets

Model Initialization:

Initialize LSTM parameters θ and optimizer with rate η_0

Set $\text{best_val_loss} \leftarrow \infty$

Training Loop:

for epoch = 1 **to** N_{ep} **do**

 Shuffle training set into mini-batches

for each batch (X_b, y_b) in training set **do**

$\hat{y}_b \leftarrow \text{LSTM}(X_b; \theta)$

$\mathcal{L} \leftarrow \frac{1}{|b|} \sum (\hat{y}_b - y_b)^2$

 Backpropagate and update θ

end for

$\hat{y}_{\text{val}} \leftarrow \text{LSTM}(X_{\text{val}}; \theta)$

$\text{val_loss} \leftarrow \frac{1}{|\text{val}|} \sum (\hat{y}_{\text{val}} - y_{\text{val}})^2$

if $\text{val_loss} < \text{best_val_loss}$ **then**

$\text{best_val_loss} \leftarrow \text{val_loss}$

$\theta^* \leftarrow \theta$

end if

 Adjust learning rate if necessary

end for

return θ^*

In this work, we employ an LSTM-based control strategy to estimate sea states based on real-time WEC measurements. The sequential nature of WEC device data, including position, velocity, and force, makes LSTM an ideal choice for capturing temporal dependencies. By leveraging memory cells, our model accurately predicts sea states without requiring external wave measurement devices. Experimental results show that our LSTM network achieved an R^2 score of 98.4% and a deployment accuracy of 94%, demonstrating its effectiveness in real-time sea state identification.

4.2. Feature Extraction

WEC parameters such as position (z), velocity (\dot{z}), and PTO force (F_{PTO}) exhibit small variations in changing wave period (T_p). Traditional time-domain approaches, such as statistical moments or signal amplitude variations, are insufficient in differentiating rapid and subtle changes in T_p . Therefore, we incorporate frequency domain features and time–frequency representations to better capture variations in ocean wave dynamics.

The Continuous Wavelet Transform (CWT) is a powerful tool for analyzing non-stationary signals by providing a joint representation in both time and frequency domains. Unlike the Fourier Transform, which decomposes a signal into pure sinusoids without time localization, CWT utilizes wavelets—localized basis functions—to capture transient and localized frequency variations [20].

Mathematically, the CWT of a signal $x(t)$ is defined as

$$W(a, b) = \int_{-\infty}^{\infty} x(t) \psi_{a,b}^*(t) dt \quad (21)$$

where $\psi_{a,b}^*(t)$ is the scaled and translated version of the mother wavelet $\psi(t)$, given by

$$\psi_{a,b}(t) = \frac{1}{\sqrt{|a|}} \psi\left(\frac{t-b}{a}\right) \quad (22)$$

Here, a represents the scale parameter, which controls the frequency resolution, and b is the translation parameter, which determines the time localization of the wavelet. The choice of the mother wavelet affects the resolution and sensitivity of the transform.

In this work, CWT is employed to extract time–frequency features from WEC measurements, enabling more accurate prediction of the wave period T_p . The wavelet coefficients $W(a, b)$ provide a multi-resolution analysis, capturing both high-frequency transient behavior and long-term variations. By integrating these features with the LSTM model, our system improves its ability to classify sea states despite small variations in T_p .

As shown in Figure 4, the first column presents the WEC position $z(t)$ in the time domain for different wave periods $T_p = 2, 3,$ and 4 s. The signals do not exhibit noticeable changes in amplitude or period at first glance. The second column displays the power spectral density (PSD), where a small variation in peak magnitude can be observed, particularly in the dominant frequency components. The third column represents the CWT-based time–frequency analysis, where distinct differences in wave energy distribution across time and frequency become evident. This highlights the advantage of using time–frequency representations in characterizing sea states, as CWT effectively distinguishes subtle changes in T_p that are not apparent in conventional time or frequency domain analyses.

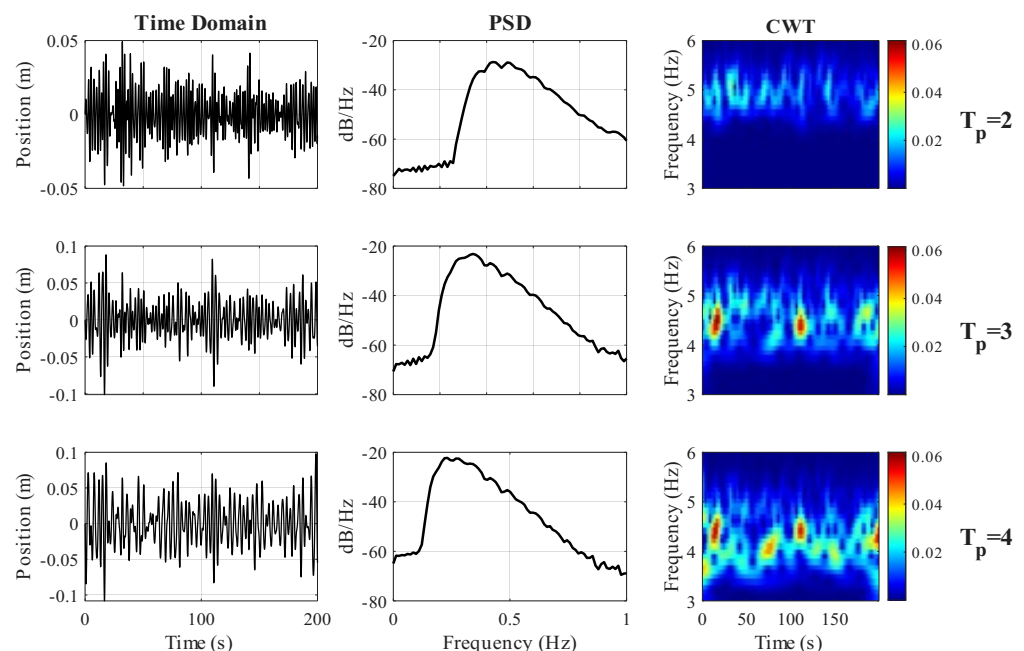


Figure 4. WEC position, $z(t)$ for different T_p in time domain (left column), frequency domain (middle column), and time–frequency domain (right column).

Several features are extracted from the WaveBot time-series data in the time domain and frequency domain. A list of features is shown in Table 2. To identify the n -best features from the WaveBot physical measurements, we introduce a composite z-score approach that integrates multiple feature evaluation metrics, providing a comprehensive measure of feature importance. Traditional feature selection methods often rely on a single criterion, which may overlook aspects of feature relevance or redundancy. Our composite z-score mitigates these limitations by combining multiple metrics, each capturing distinct aspects of feature importance.

Table 2. Selected top 10 features.

Feature	Significance	Mathematical Representation
Peak Frequency	The frequency corresponding to the maximum PSD.	$f_{\text{peak}} = \arg \max P(f)$
Spectral Centroid	Center of mass of the power spectrum.	$f_{\text{centroid}} = \frac{\sum fP(f)}{\sum P(f)}$
Spectral Flatness	Ratio of geometric mean to arithmetic mean of the power spectrum.	$F_{\text{flat}} = \frac{\exp\left(\frac{1}{N} \sum \ln P(f)\right)}{\frac{1}{N} \sum P(f)}$
Spectral Entropy	Quantifies the uniformity of spectral energy distribution.	$H = -\sum P(f) \log P(f)$
Band Power	Power in low (0–1 Hz), mid (1–3 Hz), and high frequencies.	$\int_{f_{\text{low}}}^{f_{\text{high}}} P(f) df$
Wavelet Entropy	Measures disorder in wavelet energy distribution.	$H_{\text{wavelet}} = -\sum P(s) \log P(s)$
Dominant Wavelet Scale	Scale corresponding to highest wavelet energy.	$s_{\text{dom}} = \arg \max E(s)$
Wavelet Skewness	Asymmetry of wavelet coefficients' distribution.	$\frac{\sum (W(s, t) - \mu_W)^3}{\sigma_W^3}$
Wavelet Kurtosis	Peakedness of wavelet coefficients' distribution.	$\frac{\sum (W(s, t) - \mu_W)^4}{\sigma_W^4}$
Teager Energy Operator	Captures localized energy variations in the signal.	$\sum_{n=2}^{N-1} x_n^2 - x_{n-1}x_{n+1}$

The composite z-score for each feature i , denoted as $z_{\text{composite},i}$, is defined as a weighted sum of normalized scores derived from multiple feature evaluation metrics. Let m be the number of feature evaluation methods included in the composite z-score, and let $z_{i,j}$ denote the normalized score for feature i under the j -th evaluation method. Then, the composite z-score for feature i is given by

$$z_{\text{composite},i} = \sum_{j=1}^m w_j \cdot z_{i,j} \quad (23)$$

where w_j is the weight assigned to the j -th evaluation method, with $\sum_{j=1}^m w_j = 1$. Each $z_{i,j}$ is normalized to ensure comparability across different methods and scales, typically by converting raw scores into z-scores based on the mean and standard deviation of the metric values for all features. This study uses three feature evaluation metrics to construct the composite z-score: Pearson correlation coefficient [21], variance threshold [22], and SHAP scores [23]. Each metric captures a unique aspect of feature relevance, with Pearson correlation measuring linear relationships, variance thresholding highlighting high-variance features, and SHAP scores providing model-agnostic importance based on feature contributions to predictions.

The scores from each metric are normalized to ensure comparability and then combined into a composite z-score using a weighted sum:

$$z_{\text{composite},i} = w_1 \cdot z_{i,\text{correlation}} + w_2 \cdot z_{i,\text{variance}} + w_3 \cdot z_{i,\text{SHAP}} \quad (24)$$

where w_1 , w_2 , and w_3 are weights assigned to each metric, with $w_1 + w_2 + w_3 = 1$. The weights are selected based on cross-validation performance to ensure optimal feature selection for our specific model and data.

After calculating $z_{\text{composite}}$ for each feature, the top 10 features with the highest $z_{\text{composite}}$ values are selected as the final feature set. This composite z-score approach demonstrates improved robustness and interpretability compared to single-metric feature selection as shown in our empirical results in Section 4.

5. Result Analysis

5.1. Model Training

In the first stage, the WaveBot device is simulated in MATLAB/Simulink (Version 24.1) to generate device position (z), velocity (\dot{z}), and PTO force (F_{PTO}). A wide range of JONSWAP spectra is used to mimic real-life ocean conditions. Wave heights of $H_m \in [1, 6]$ m and peak periods of $T_p \in [8, 15]$ s are suitable for Pacific Northwest sea conditions. Therefore, a full-scale T_p ranging from 1 to 15 s is used to generate the WaveBot physical data. Since we are using a 1/17th scaled version of the original WaveBot device, we apply similar scaling to the input wave characteristics, H_m and T_p .

During training, wave excitation force, F_{exc} is generated using wave surface elevation profiles for $T_p \in [1, 4]$ s, $H_m = 0.127$ m, and the hydrodynamic properties of the WaveBot device. A time step of 0.01 s is used to generate device data that are later used to train the LSTM model. The choice of window size and *step size* in feature extraction plays a critical role in effectively capturing the underlying dynamics of the WEC. In this study, we select a sampling frequency of 100 Hz, meaning that each recorded second contains 100 data points. To ensure that the extracted features encapsulate meaningful temporal variations, a window size of 1000 samples is chosen, equivalent to 10 s of data per window. This 10-second duration is sufficiently long to capture the dominant wave characteristics and WEC response while balancing computational efficiency. Given that ocean waves exhibit characteristic periods ranging from a few seconds to over a dozen seconds, this window size ensures that at least one full wave cycle is included in each window, even for the longest wave periods in the dataset.

For model training, wave periods (T_p) between 1 and 4 s are used, covering a wide range of dynamically different sea states. In all cases, the wave height (H_m) and the peak enhancement factor (γ) are fixed at 0.127 m and 1, respectively. We have used Python 3.10 along with TensorFlow 2.11.0 to build, train, and test the LSTM-based neural network model. A list of model architecture is shown in Table 3.

Table 3. LSTM model architecture.

Parameter	Value
Loss Function	MSE
Optimizer	Adam
Number of Layers	2
Neurons per Layer	50, 50
Dropout	0.2
Batch Size	32
Epochs	50
Learning Rate	0.001
Activation Function	ReLU

Figure 5 illustrates the comparison between predicted and actual peak period (T_p) values. The black scatter points represent the LSTM model's predictions, while the red dashed line corresponds to the ideal one-to-one fit. The close alignment of most data points along this line indicates strong predictive performance. The model achieves a coefficient of determination (R^2 -score) of 98.4%, demonstrating its ability to capture the underlying wave dynamics with high accuracy. Even on test data with T_p values extending beyond the training range, the model maintains strong predictive capability, highlighting its generalization performance. Minor deviations from the ideal fit can be seen due to inherent noise in wave conditions and model uncertainties. However, the overall trend confirms that the LSTM-based approach effectively learns the nonlinear relationships between

wave excitation forces and device responses, making it a reliable choice for real-world WEC applications.

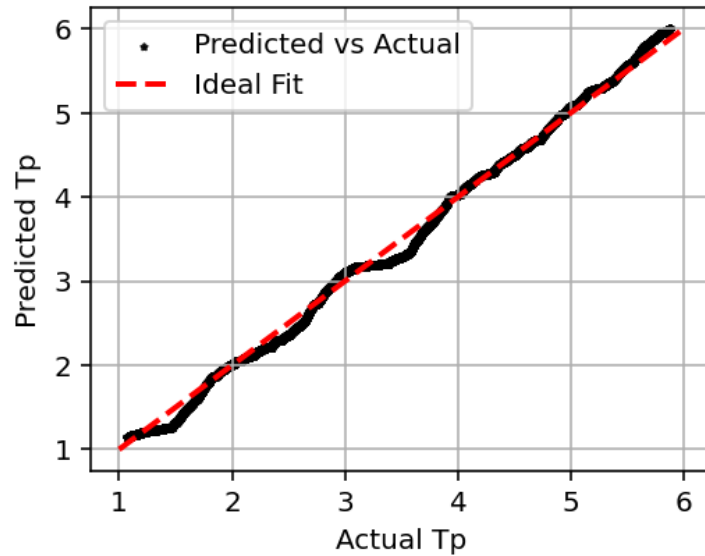


Figure 5. LSTM model prediction.

5.2. Fixed Sea State: Prediction and Control

The trained LSTM model is employed within the control loop via MATLAB-Python co-design integration. As a supervisory control, the trained LSTM model predicts the incoming wave period, T_p , based on WaveBot measurements (z, \dot{z}, F_{PTO}) , which is then used to determine and apply the proportional and integral gains K_P and K_I . Predicted T_p is normalized since Min-Max scaling is applied during training. Therefore, it is scaled back to its original form using the Min-Max values of the features.

Figures 6 and 7 present the simulation results from MATLAB/Simulink, demonstrating the effectiveness of the trained LSTM model in real-time wave prediction, and control applied based on that prediction. The first subplot of Figure 6 shows the setting of the fixed period case, in which the control parameters are set based on the accurate prediction of a 5 s sea state, and the prediction of the sea state based on observations of the system response. The subsequent plots display the variations in control parameters, K_P and K_I , which adapt dynamically based on the predicted T_p . Note that K_I gain is limited to -2×10^4 due to the device constraint as shown in Table 1. The position, velocity, and PTO force (F_{PTO}) plots further illustrate the system’s response to the incoming waves. Figure 7 illustrates the average power captured over time for two control approaches.

The PTO power $P_{PTO}(t)$ is computed using the instantaneous PTO force $F_{PTO}(t)$ and the velocity of the device $\dot{z}(t)$. The instantaneous PTO power is given by

$$P_{PTO}(t) = F_{PTO}(t) \cdot \dot{z}(t). \tag{25}$$

The average power P_{avg} is then computed by dividing the total extracted energy by the total time duration T :

$$P_{avg} = \frac{1}{T} \int_0^T P_{PTO}(t) dt. \tag{26}$$

In conventional control strategies, T_p remains constant, potentially limiting adaptability to changing wave conditions. In contrast, our approach updates T_p every 10 s based on real-time responses from the WaveBot device. This adaptation leads to a more responsive control strategy, yielding improved power capture. The results show that the proposed

method achieves an average power of 36.65 W, compared to 35.26 W with the fixed T_p , slightly improving power capture compared to the fixed T_p approach.

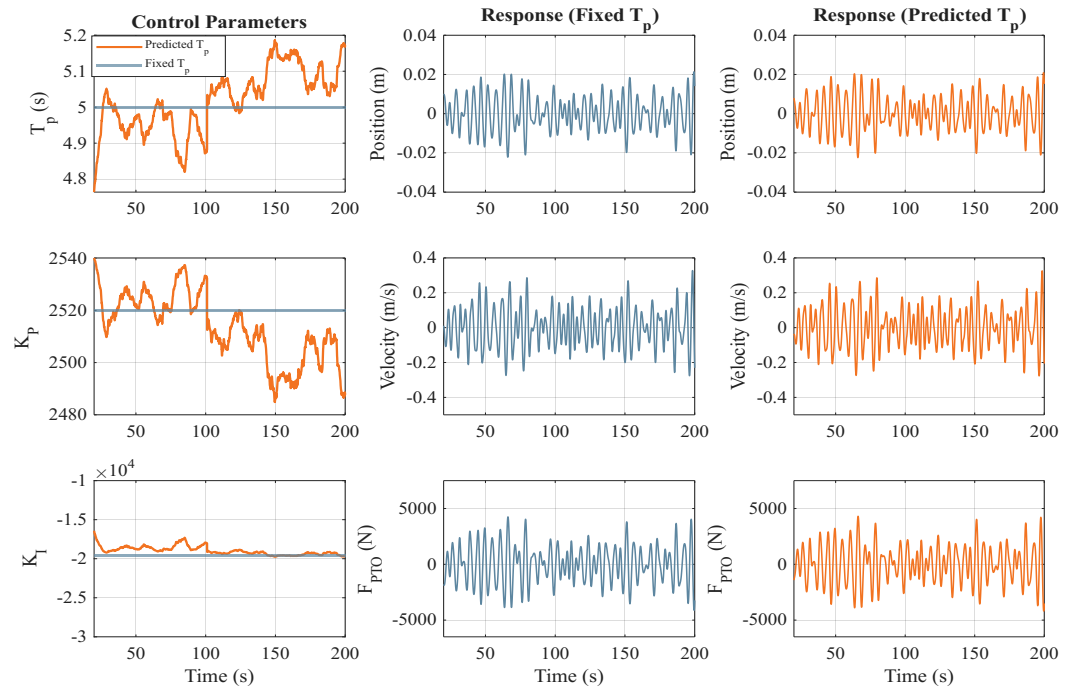


Figure 6. Simulation results for a $T_p = 5$ s sea state. The blue traces are for control, applied assuming a fixed $T_p = 5$ s sea state. The orange traces are for adaptive control, in which the period is predicted based on device motion and performance.

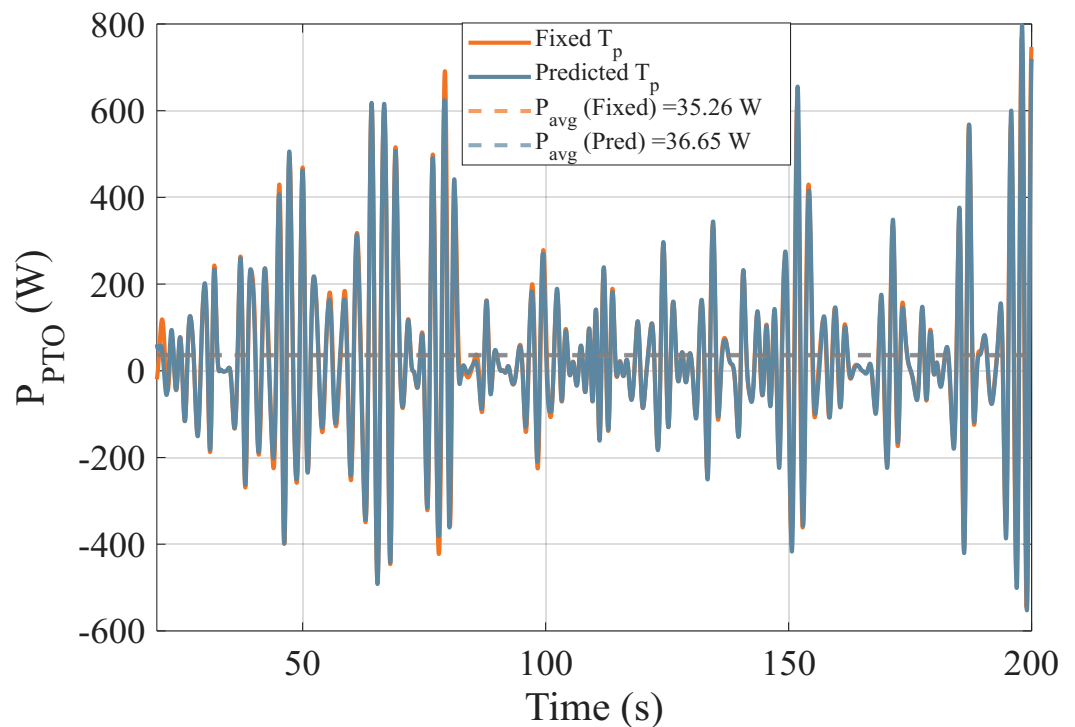


Figure 7. Instantaneous and average power over for $T_p = 5$ s. The performance, in terms of average power, is as expected, with both control approaches being approximately equal in performance.

5.3. Variable Sea State: Prediction and Control

The water surface elevation function $\eta(t)$ is constructed as

$$\eta(t) = \sum_{i=1}^N \sqrt{2S_c(\omega_i, t)} \sin(\omega_i t + \phi_i) \tag{27}$$

where ω_i is the angular frequency, ϕ_i is a random phase uniformly distributed in $[0, 2\pi]$, and $S_c(\omega, t)$ is the time-dependent wave spectrum transitioning between two sea states:

$$S_c(\omega, t) = \frac{5\pi^4 H_s(t)^2}{T_p(t)^4 \omega^5} \exp\left(\frac{-20\pi^4}{T_p(t)^4 \omega^4}\right) \tag{28}$$

$$H_s(t) = m_1(t)H_{s1} + m_2(t)H_{s2}, \tag{29}$$

$$T_p(t) = m_1(t)T_{p1} + m_2(t)T_{p2}, \tag{30}$$

where the time-dependent mixing coefficients are given by

$$m_1(t) = 1 - \frac{t}{t_{\text{end}}}, \quad m_2(t) = \frac{t}{t_{\text{end}}}. \tag{31}$$

This ensures a smooth transition from sea state 1 at $t = 0$ to sea state 2 at $t = t_{\text{end}}$. The resulting wave elevation function $\eta(t)$ accurately represents a dynamically evolving sea state.

Figure 8 presents the WEC motion response under a dynamically varying wave period T_p ranging from 2 s to 6 s. The left column displays the control parameters: the estimated period T_p , proportional gain K_P , and integral gain K_I , while the right column illustrates the WaveBot device response in terms of position, velocity, and PTO force over time. In the first column, it is evident that the predicted period approach is tracking the changing sea state and adjusting the proportional and integral gains accordingly.

Figure 9 illustrates the average power capture over time for two control approaches: a fixed T_p of 4 s (conventional method) and a dynamically predicted T_p . Unlike the fixed approach, where T_p remains constant, the proposed method adaptively updates T_p based on real-time responses from the WaveBot device, enabling the continuous tuning of the proportional gain K_P and integral gain K_I . The results demonstrate a significant improvement in power capture with the adaptive approach. The proposed method achieves an average power of 34.09 W, compared to 27.13 W with the fixed T_p . This demonstrates a 25.6% increase in power capture compared to the fixed T_p approach. This increase in power extraction efficiency is attributed to the real-time adjustment of control parameters, which allows the WEC to better synchronize with incoming wave conditions. By dynamically optimizing K_P and K_I , the system effectively maximizes energy conversion, validating the advantage of adaptive control over traditional fixed-gain strategies.

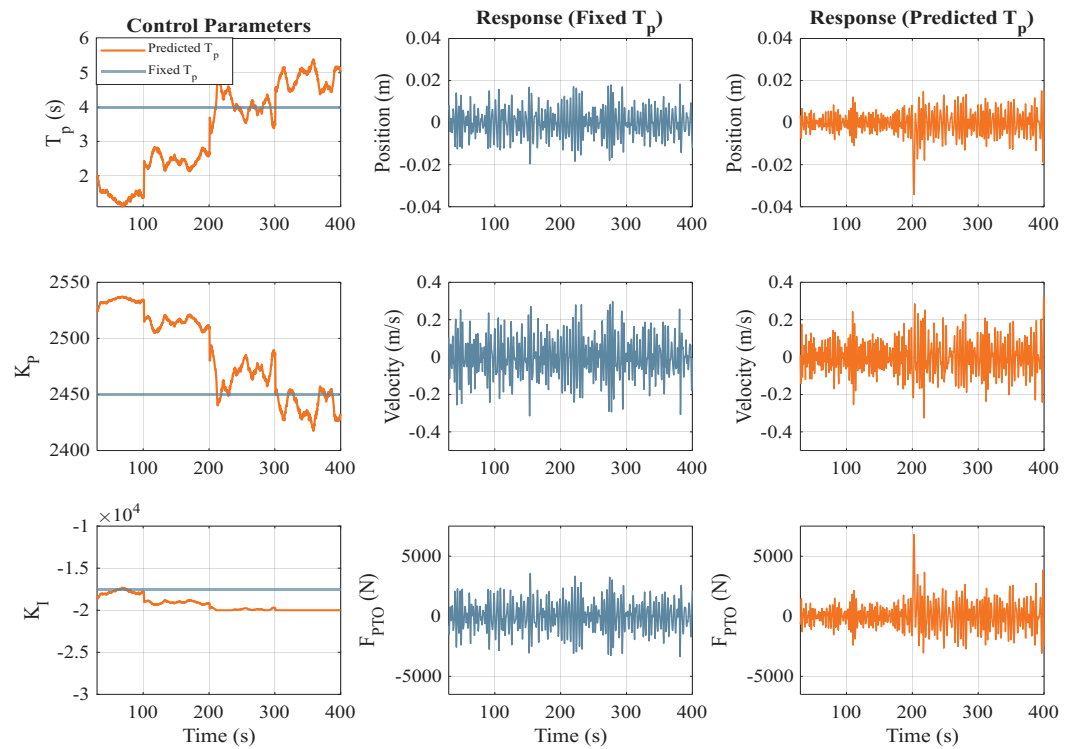


Figure 8. WaveBot performance in variable sea states, $T_p \in [2, 6]$. The sea state linearly varies over the 400 s simulation time, starting at 2 s period and ending at 6 s period.

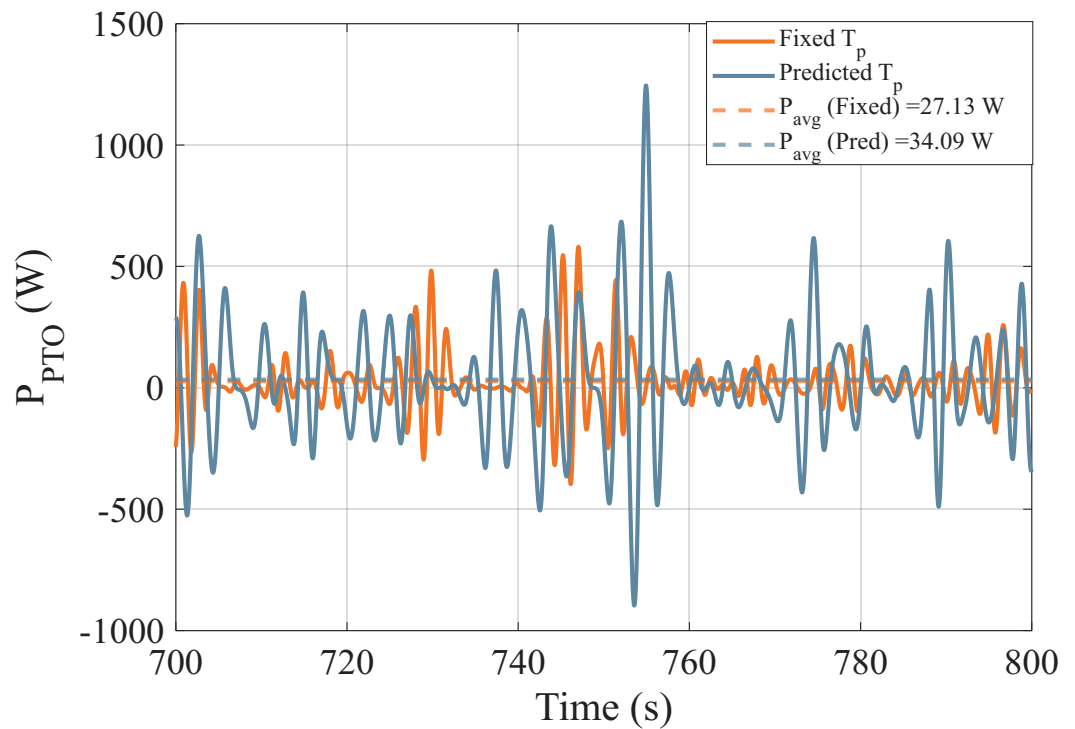


Figure 9. Instantaneous and average power produced by fixed $T_p = 4$ and variable $T_p \in [2, 6]$. The instantaneous sea state period detection approach significantly outperforms the fixed case by 34.09 W average power to 27.13 W.

6. Discussion

Our proposed control approach is compared with several other traditional machine learning models and control strategies. Table 4 presents a comparative analysis of different models for both fixed and variable T_p , emphasizing the effectiveness of the proposed

LSTM-based control technique. The results demonstrate that LSTM outperforms ANN and SVR across all performance metrics, achieving the highest R^2 -score and the lowest RMSE for both cases. For the fixed T_p scenario, LSTM attains an R^2 -score of 0.98 with an RMSE of 0.005, leading to an average power capture (P_{avg}) of 35.26 W, the highest among all models. Similarly, under the variable T_p approach, LSTM maintains superior performance with an R^2 -score of 0.96 and an RMSE of 0.03, achieving an average power capture of 34.09 W. This power capture outperforms the baseline PI controller, which yields 27.13 W. The key outcome of this study is the demonstrated effectiveness of the LSTM-based control approach in adapting to varying sea states. Conventional PI control with fixed K_P and K_I struggles with dynamic wave conditions, showing similar power capture in fixed sea states but poor performance in variable sea states. However, the proposed method dynamically adjusts control parameters, leading to enhanced power extraction. These results validate the potential of machine learning-driven adaptive control strategies in optimizing energy capture for wave energy converters. The proposed LSTM model demonstrates promising results in predicting ocean wave parameters from WaveBot measurements; however, certain limitations remain. One of the major challenges is the MATLAB-Python co-design integration, which requires specific version compatibility for both training and testing phases. Also, the addition of AWGN to the WaveBot measurements can cause discrepancies, especially at peak force amplitudes; hence, the model's sensitivity to noise intensity requires further investigation.

Table 4. Comparison of different models for fixed and variable T_p .

Model	Fixed T_p			Variable T_p		
	R^2 -Score	RMSE	Pavg (W)	R^2 -Score	RMSE	Pavg (W)
ANN	0.95	0.02	35.6	0.92	0.04	33.11
SVR	0.89	0.09	34.21	0.87	0.15	31.86
LSTM	0.98	0.005	36.65	0.96	0.03	34.09
Baseline (PI)	-	-	35.26	-	-	27.13

Future work could address these limitations by exploring alternative noise models, such as colored noise, to better simulate oceanic environments. Additionally, we plan to leverage direct CWT images as inputs to train CNNs for improved feature extraction and wave parameter predictions. Pretrained CNN models will also be explored to enhance the accuracy and efficiency of T_p estimation, leveraging transfer learning techniques for better generalization across varying sea states. Furthermore, integrating the model with real-time data acquisition from WaveBot could provide insights into practical implementation challenges and further optimize performance for live ocean energy applications. Addressing these directions would improve the model's robustness, generalizability, and practical value in ocean wave prediction and energy harvesting.

7. Conclusions

This study presented an LSTM-based approach for predicting sea states by utilizing features extracted from a WEC device's physical measurements. Later, a MATLAB-Python co-design architecture is used to integrate wave predictions with a PID controller to obtain optimal control actions that maximize energy extraction. The results show that the proposed control approach significantly enhances power capture in both fixed and variable sea conditions. For the fixed sea state case, the proposed method captures the same amount of power as the traditional fixed T_p approach, which is optimally tuned for that particular T_p . In the variable sea state scenario, the model was able to tune PID controller gains based on the real-time wave conditions. This adaptation improved power capture by

25.6%, demonstrating the effectiveness of the real-time tuning of K_p and K_i using the LSTM-predicted sea states. By leveraging these improvements, our proposed method can offer a practical, resilient solution for WEC control by focusing on device measurements, thereby reducing the need for complex and costly wave predictions.

Author Contributions: Conceptualization, T.A.S. and T.B.; methodology, T.B. and R.C.; software, T.A.S.; validation, R.C., G.B. and T.B.; formal analysis, T.A.S.; investigation, T.B.; resources, T.B. and R.C.; data curation, T.A.S.; writing—original draft preparation, T.A.S.; writing—review and editing, T.B. and R.C.; visualization, T.A.S.; supervision, T.B.; project administration, R.C. and G.B.; funding acquisition, T.B. All authors have read and agreed to the published version of the manuscript.

Funding: This research was funded by Sandia National Laboratory under DOE Water Power Technologies Office DE-NA0003525.

Institutional Review Board Statement: Not applicable.

Informed Consent Statement: Not applicable.

Data Availability Statement: The data presented in this study are available on request from the corresponding author. The data are not publicly available due to privacy.

Acknowledgments: Sandia National Laboratories is a multi-mission laboratory managed and operated by National Technology and Engineering Solutions of Sandia, LLC., a wholly owned subsidiary of Honeywell International, Inc., for the U.S. Department of Energy’s National Nuclear Security Administration under contract DE-NA0003525. This paper describes objective technical results and analysis. Any subjective views or opinions that might be expressed in the paper do not necessarily represent the views of the U.S. Department of Energy or the United States Government.

Conflicts of Interest: The authors declare no conflicts of interest.

Abbreviations

The following abbreviations are used in this manuscript:

ANN	Artificial Neural Network
AWGN	Additive White Gaussian Noise
CF	Crest Factor
CCC	Complex Conjugate Control
CWT	Continuous Wavelet Transform
DNN	Deep Neural Network
FBR	Feedback Resonating Control
LSTM	Long Short-Term Memory
MPC	Model Predictive Control
PI	Proportional–Integral
PTO	Power Take-Off
RNN	Recurrent Neural Network
SHAP	SHapley Additive exPlanations
SVR	Support Vector Regression
T_p	Peak Wave Period
WEC	Wave Energy Converter

Nomenclature

Symbols and definitions used throughout the manuscript.

Symbol	Definition	Unit
m	Mass of the WEC	kg
k_h	Hydrostatic stiffness	N/m
b_f	Frictional damping coefficient	N·s/m
N	Gear ratio	rad/m
J_d	Rotor (shaft) inertia	kg·m ²
k_τ	Motor torque constant	N·m/A
R_w	Motor winding resistance	Ω
α	Phillips parameter (JONSWAP)	—
g	Gravitational acceleration	m/s ²
ω	Angular frequency	rad/s
ω_p	Peak angular frequency	rad/s
γ	JONSWAP peak enhancement factor	—
σ	Spectral width parameter	—
$x[k]$	State vector at discrete time step k	—
$u[k]$	Input vector at discrete time step k	—
A, B, C, D	State-space matrices	—
$H(z)$	Discrete-time transfer function	—
T_s	Sampling period	s
$z(t)$	Vertical displacement of the WEC	m
$\dot{z}(t)$	Vertical velocity of the WEC	m/s
$F_{PTO}(t)$	Power-take-off force	N
K_p	Proportional gain	N·s/m
K_I	Integral gain	N·s ² /m
f_{peak}	Frequency at peak of PSD	Hz
f_{centroid}	Spectral centroid	Hz
F_{flat}	Spectral flatness	—
H_{spectral}	Spectral entropy	—
P_{band}	Band power in specified frequency ranges	—
s	CWT scale parameter	—
b	CWT translation (time shift)	s
$\psi(t)$	Mother wavelet	—
$W(a, b)$	Continuous wavelet coefficient	—

References

- Zhang, Y.; Zhao, Y.; Sun, W.; Li, J. Ocean wave energy converters: Technical principle, device realization, and performance evaluation. *Renew. Sustain. Energy Rev.* **2021**, *141*, 110764. [\[CrossRef\]](#)
- Fusco, F.; Ringwood, J.V. A predictive control strategy for wave energy conversion in irregular waves. *IEEE Trans. Sustain. Energy* **2010**, *1*, 92–99.
- Henriques, J.C.C.; Neves, S.P.; Guedes, R.T.; Falcão, A.F.O. Model predictive control of a floating oscillating water column wave energy converter. *Renew. Energy* **2016**, *85*, 170–182. [\[CrossRef\]](#)
- Falnes, J. *Ocean Waves and Oscillating Systems: Linear Interactions Including Wave-Energy Extraction*; Cambridge University Press: Cambridge, UK, 2002.
- Li, G.; Belmont, M.R. Model predictive control of sea wave energy converters—Part I: A convex approach for the case of a single device. *Renew. Energy* **2014**, *69*, 453–463. [\[CrossRef\]](#)
- Coe, R.G.; Bacelli, G.; Nevarez, V.; Cho, H.; Wilches-Bernal, F. *A Comparative Study on Wave Prediction for WECs*; Sandia National Laboratories Report; Sandia National Laboratories (SNL-NM): Albuquerque, NM, USA, 2018; SAND2018-8603.
- Yu, Z.; Falnes, J. State-space modelling of a vertical cylinder in heave. *Appl. Ocean Res.* **1995**, *17*, 265–275. [\[CrossRef\]](#)
- Vantorre, M.; Verhoeven, P.; Frigaard, A. Wave energy devices with mechanical energy storage. In Proceedings of the International Conference on Offshore Mechanics and Arctic Engineering, Vancouver, BC, Canada, 20–25 June 2004; Volume 4, pp. 241–248.
- Gelb, A. *Applied Optimal Estimation*; MIT Press: Cambridge, MA, USA, 1974.

10. Simon, D. *Optimal State Estimation: Kalman, H_∞ and Nonlinear Approaches*; Wiley-Interscience: Hoboken, NJ, USA, 2006.
11. Julier, S.J.; Uhlmann, J.K. A new extension of the Kalman filter to nonlinear systems. In Proceedings of the AeroSense '97 (SPIE 3068), Orlando, FL, USA, 21 April 1997; pp. 182–193.
12. Doucet, A.; de Freitas, N.; Gordon, N. *Sequential Monte Carlo Methods in Practice*; Springer: New York, NY, USA, 2000.
13. Anderson, B.D.O.; Moore, J.B. *Optimal Control: Linear Quadratic Methods*; Dover Publications: Mineola, NY, USA, 2007.
14. Zou, Y.; Wang, Y.; Zhang, X. Neural network-based resource prediction and optimization for renewable energy systems. *Appl. Energy* **2017**, *206*, 1024–1035.
15. He, Y.; Zuo, L. Machine learning for reliability assessment and lifetime prediction of wave energy converters. *Ocean Eng.* **2021**, *235*, 109443.
16. Li, H.; Zhao, J.; Chen, P. Deep learning for wave energy prediction and WEC optimization. *Renew. Energy* **2020**, *147*, 1689–1701.
17. Duarte, A.; Sarmiento, A. Machine learning for wave energy conversion. In Proceedings of the 12th European Wave and Tidal Energy Conference, Cork, Ireland, 27 August–1 September 2017.
18. Cho, H.; Bacelli, G.; Coe, R.G. Model Predictive Control Tuning by Inverse Matching for a Wave Energy Converter. *Energies* **2019**, *12*, 4158. [[CrossRef](#)]
19. Olah, C. Understanding LSTM Networks. *colah's blog*, 27 August 2015. Available online: <https://colah.github.io/posts/2015-08-Understanding-LSTMs/> (accessed on 11 May 2025).
20. Lilly, J.M. Element Analysis: A Wavelet-Based Method for Analysing Time-Localized Events in Noisy Time Series. *Proc. R. Soc. A Math. Phys. Eng. Sci.* **2017**, *473*, 20160776. [[CrossRef](#)] [[PubMed](#)]
21. Cohen, I.; Huang, Y.; Chen, J.; Benesty, J.; Benesty, J.; Chen, J.; Huang, Y.; Cohen, I. Pearson correlation coefficient. In *Noise Reduction in Speech Processing*; Springer: Berlin/Heidelberg, Germany, 2009; pp. 1–4.
22. Hou, Z.; Hu, Q.; Nowinski, W.L. On minimum variance thresholding. *Pattern Recognit. Lett.* **2006**, *27*, 1732–1743. [[CrossRef](#)]
23. Van den Broeck, G.; Lykov, A.; Schleich, M.; Suci, D. On the tractability of SHAP explanations. *J. Artif. Intell. Res.* **2022**, *74*, 851–886. [[CrossRef](#)]

Disclaimer/Publisher's Note: The statements, opinions and data contained in all publications are solely those of the individual author(s) and contributor(s) and not of MDPI and/or the editor(s). MDPI and/or the editor(s) disclaim responsibility for any injury to people or property resulting from any ideas, methods, instructions or products referred to in the content.